



UDC 621.762.2

<https://doi.org/10.17073/1997-308X-2024-1-81-94>Research article
Научная статья

Mechanical properties of high-nitrogen steel produced via selective laser melting using mechanically alloyed and spheroidized powders

N. E. Ozerskoi , N. G. Razumov, A. O. Silin,
E. V. Borisov, A. A. Popovich

Peter the Great St. Petersburg Polytechnic University
29 Polytekhnicheskaya Str., St. Petersburg 195251, Russian Federation

 nikolaiozerskoi@yandex.ru

Abstract. In recent years, the development of additive technologies has been one of the priority tasks in the sector. Primarily, additive technologies enable the effective implementation of various design and engineering ideas in high-tech industries, such as the aircraft industry, engine technology, and rocket engineering. The expanded range of standardized materials for additive technologies will facilitate their integration into large-scale production. Of significant interest is the potential use of nitrogen-containing heat-resistant powder alloys to produce complex-shaped aircraft parts using additive technologies. This paper describes the complete process of obtaining samples from powders of alloys with superequilibrium nitrogen content using the selective laser melting (SLM) method. Four different compositions of high-nitrogen steels were obtained through mechanical alloying. Subsequently, the powders of these steels underwent processing using the plasma spheroidization method to be utilized in the SLM process. The SLM method was also employed to produce samples for mechanical tests. Throughout each stage of the process, the powders were thoroughly analyzed. One of the most critical parameters was the nitrogen content in the resulting powders. At each subsequent production stage, its proportion decreased, yet it remained at the superequilibrium content level of 0.13–0.44 wt. %. The mechanical tests confirmed that the alloys fabricated by the SLM method are not inferior in terms of their properties compared to those obtained using classical metallurgical technologies.

Keywords: high-nitrogen steels, superequilibrium nitrogen content, plasma spheroidization, mechanical alloying, additive technologies, selective laser melting

For citation: Ozerskoi N.E., Razumov N.G., Silin A.O., Borisov E.V., Popovich A.A. Mechanical properties of high-nitrogen steel produced via selective laser melting using mechanically alloyed and spheroidized powders. *Powder Metallurgy and Functional Coatings*. 2024;18(1):81–94. <https://doi.org/10.17073/1997-308X-2024-1-81-94>

Механические свойства стали с высоким содержанием азота, полученной методом селективного лазерного плавления с использованием механически легированных сфероидизированных порошков

Н. Е. Озерской , Н. Г. Разумов, А. О. Силин,
Е. В. Борисов, А. А. Попович

Санкт-Петербургский политехнический университет Петра Великого
Россия, 195251, г. Санкт-Петербург, ул. Политехническая, 29

nikolaiozerskoi@yandex.ru

Аннотация. В последние годы развитие аддитивных технологий является одной из приоритетных задач отраслей. Аддитивные технологии позволяют, прежде всего, эффективно реализовывать любые конструкторские и инженерные идеи в таких высокотехнологичных отраслях, как авиастроение, двигателестроение, ракетостроение. Расширение номенклатуры стандартизованных материалов для аддитивных технологий будет способствовать их внедрению в массовое производство. Значительный интерес представляет возможность использования азотсодержащих жаропрочных порошковых сплавов для изготовления деталей летательных аппаратов сложной формы с применением аддитивных технологий. В данной работе описан полный цикл получения образцов из порошков сплавов со сверхравновесным содержанием азота методом селективного лазерного плавления (СЛП). Механическим легированием были получены 4 различных состава высокоазотистых сталей. Затем порошки этих сталей были обработаны методом плазменной сфероидизации для использования в процессе СЛП. Также методом СЛП были изготовлены образцы для механических испытаний. На каждом этапе процесса порошки подвергались детальному исследованию. Одним из наиболее важных параметров было содержание азота в получаемых порошках. С каждым этапом производства его доля снижалась, но оставалась на уровне сверхравновесного содержания 0,13–0,44 мас. %. Механические испытания показали, что сплавы, полученные методом СЛП, не уступают по своим свойствам сплавам, изготовленным по классическим металлургическим технологиям.

Ключевые слова: высокоазотистые стали, сверхравновесное содержание азота, плазменная сфероидизация, механическое легирование, аддитивные технологии, селективное лазерное плавление

Для цитирования: Озерской Н.Е., Разумов Н.Г., Силин А.О., Борисов Е.В., Попович А.А. Механические свойства стали с высоким содержанием азота, полученной методом селективного лазерного плавления с использованием механически легированных сфероидизированных порошков. *Известия вузов. Порошковая металлургия и функциональные покрытия*. 2024;18(1): 82–94. <https://doi.org/10.17073/1997-308X-2024-1-81-94>

Introduction

Currently, nitrogen is extensively utilized as an alloying element alongside Cr, Ni, Mn, Mo, and others [1]. This usage enables the production of steels with a distinctive blend of strength, ductility, and corrosion resistance. Nitrogen possesses a critical advantage over other alloying elements due to its virtually unlimited availability. Obtaining nitrogen does not necessitate the destruction of the Earth's surface and subsoil, which is typically unavoidable during ore mining.

Presently, research on steels alloyed with nitrogen, focusing on structure formation and the interrelationships of steel properties with nitrogen, has generated significant results, leading to the proposal of new areas for their application [2–5]. Owing to their exceptional properties, nitrogen-containing steels have found widespread use in nuclear and thermal power engineering, the medical industry, aviation, the automotive industry,

and more. Nitrogen alloying has the capability to confer special properties to steel and enhance its characteristics, thereby broadening its scope of applications. As of now, the full potential of nitrogen alloying remains unrealized, and research in this field continues.

The literature review reveals active scholarly investigations into the potential use of nitrogen-containing steels in various additive technologies (AT). Numerous studies have been published examining the testing of nitrogen-containing steels in selective laser melting (SLM) [6; 7], laser powder bed fusion (LPBF) [8–15], wire and arc additive manufacturing (WAAM) [16–19], and electron beam additive manufacturing (EBAM) [20–22]. Each technology possesses its distinct characteristics and features.

Studies [6; 7] emphasize that nitrogen emission occurs during the SLM of nitrogen-containing stainless steels. The emission levels correlate with the energy den-

sity, which is directly proportional to the laser power and inversely proportional to the scanning speed. Investigations [9–14] demonstrate the potential use of powders of nitrogen-containing steels in LPBF technology. They indicate that regardless of the process gas used to feed the powder into the melt pool, the nitrogen content decreases. Higher melt pool temperatures reduce nitrogen solubility in the melt, resulting in degassing and the formation of gas pores. Moreover, a study [15] illustrates that during LPBF, local changes in the geometry of the melt pool, influenced by energy density, can affect nitrogen emission. Elevated energy densities lead to prolonged melt pool lifetimes and higher maximum liquid phase temperatures. Assuming that nitrogen is primarily lost during the melting stage, increased maximum temperatures and extended lifetimes of the melt pool contribute to nitrogen loss. With increased energy density, the size of the melt pool – its depth and area – along with its temperature and lifetime also increase.

The paper [19] introduces a novel concept in wire and arc additive manufacturing aimed at achieving pure austenite with an exceptionally high nitrogen content. This technique involves the simultaneous introduction of nitrogen-containing steel welding wire and nitride alloy powder into the melt pool. As the nitride powder dissolves within the melt pool, it dissociates and is adsorbed to create steel with a superequilibrium nitrogen content. The authors highlight that during the wire and arc additive manufacturing process utilizing HNS6 wire (Fe–21.6Cr–16.8Mn–2.1Ni–1.2Mo–0.8N), there is a recorded nitrogen loss rate of up to 17.7 %. However, in hybrid wire and arc additive manufacturing, where nitride powder is introduced into the melt pool, the nitrogen content in the resultant material increases significantly, potentially reaching 1.07 wt. % based on the powder feed rate. Concurrently, there is a substantial reduction in ferrite content. As the feed rate reaches 0.33 g/min, the ferrite phase disappears entirely, resulting in a fully austenitic structure in the deposited metal. This transformation contributes to the enhancement of the material's mechanical properties.

The paper [20] details the successful application of the electron-beam additive method to produce high-nitrogen steel with the chemical composition: Fe–20.7Cr–22.2Mn–0.3Ni–0.6Si–0.15C–0.53N (wt. %), utilizing rods as the initial material. The authors demonstrate that during the manufacturing process, significant amounts of manganese and nitrogen undergo combustion. Consequently, the alloy obtained, with the composition Fe–22.9Cr–10.8Mn–0.1Ni–0.6Si–0.1C–0.48N, exhibits an increased proportion of ferrite, rising from 20 % in the initial rod to 40 % in the alloy produced via additive technologies (AT). Their findings indi-

cate that alloys generated using both AT and traditional methods possess comparable mechanical characteristics.

The primary method for producing nitrogen-containing steel powders is through gas atomization [6; 7; 9; 13; 14; 22–24]. The nitrogen content in these resultant powders typically does not surpass the equilibrium level and is contingent upon the specific alloy composition. Nevertheless, several researchers have explored the possibility of producing steel powders with nitrogen content surpassing equilibrium levels. In a study by the authors [25], the impact of various factors – such as atmosphere composition, chamber pressure, and gas jet pressure – during atomization on the nitrogen content in Cr17Mn11Mo3N alloy powder was investigated. The research demonstrated that the nitrogen proportion in atomized powders escalates as the pressure in the chamber increases during the melting and spraying process. Through the combined effect of chamber pressure during melting and spray pressure, the nitrogen content can reach up to 0.4 wt. % even in the absence of nitrogen-containing components added to the charge. The findings suggested that by regulating the spray pressure and/or pressure in the chamber, it is feasible to control both the powder particle size and the nitrogen content in the resultant powders.

The paper [26] presents findings from research involving the production of 17-4PH stainless steel powder using plasma wire atomization. The authors successfully produced powder with a nitrogen content of up to 0.15 wt. %, which was then utilized in the SLM technology.

In the paper [27], the production of high-nitrogen steel powders through plasma spraying of a rotating electrode is detailed. The resulting powder exhibited a notably high nitrogen content, surpassing levels achievable under normal conditions, and displayed an almost perfect spherical particle shape. Notably, in a nitrogen atmosphere during plasma spraying, the nitrogen content in the steel powders remained consistently at approximately 0.6 wt. % N, regardless of the nitrogen content in the plasma gas itself. It was observed that even when the nitrogen content in the plasma gas is 0 %, the steel becomes nitrogenized to 0.6 wt. % N. This occurrence is attributed to the interaction between the argon plasma and the surrounding nitrogen gas, which is sufficient for nitrogen sorption onto the steel particles.

The papers [28; 29] detail the process involving powders of AISI 316L and Fe17Cr11Mn3Mo alloys obtained through gas atomization and subsequently nitrogenized in a nitrogen atmosphere under pressure. The research demonstrates that, based on the nitrogenizing duration and powder composition, powders with nitrogen content up to 1.3 wt. % can be achieved.

Analysis indicates that this elevated nitrogen content is attained due to the formation of chromium nitride both on the surface and throughout the cross-section of the powder particles. However, this process is characterized as low-yielding, and there exists an issue concerning the homogeneity of nitrogen content across the particles.

The LPBF technology as described in paper [8], allows the utilization of non-spherical-shaped powder materials. High-nitrogen austenitic steel derived from powder synthesized by mechanical alloying (MA) is explored in this context. The study demonstrates that the alloy retains more than 71 % of the initial powder mixture's nitrogen content. Remarkably, this material surpasses 316L steel significantly in terms of mechanical properties.

Furthermore, in the additive technology (AT) process of welding steels with high nitrogen content, there's a tendency for nitrogen to be released in the melt pool, resulting in diminished mechanical characteristics of the final products. Researchers have been exploring various methods over the last few decades to increase nitrogen content in the solid solution in deposited material and reduce loss due to nitride or pore formation. These methods include optimizing the chemical composition to enhance nitrogen solubility [30–33], modifying shielding gas characteristics by increasing nitrogen partial pressure [34–37] or adding surfactants [38] or multi-component gas mixtures [39] during welding, and using nitride flux-cored wire as feed material [40; 41]. While these approaches can reduce nitrogen loss during steel welding to some extent, the nitrogen content in the weld or deposited metal remains lower than that in the base or filler metal. Thus far, no solution has been presented to increase the nitrogen content in the deposited metal or weld beyond that of the filler or base metal.

Based on the outlined objectives, the following research is proposed: 1) establishing physical and chemical synthesis patterns of metallic nitrogen-containing heat-resistant powder alloys via MA and plasma spheroidization methods; 2) determining the influence of physical and chemical parameters within the SLM process on the nitrogen content of the alloy and evaluating the resulting material's mechanical properties.

This investigation will focus on studying a specific heat-resistant nitrogen-containing steel, Fe16Cr2.2Ni0.6Mn1.1Mo0.1N, with the following chemical composition, wt. %:

Fe	Base	Ni	2.0–2.5
Cr	15.0–16.5	C	0.12–0.18
Mo	0.9–1.3	Si	≤0.6
Mn	≤0.6	N	0.03–0.10

Materials and methods

In this research, powder materials of the composition Fe–16Cr–2.2Ni–0.6Mn–1.1Mo were synthesized using the MA method. Gaseous nitrogen, nitrogenized ferrochrome (FCr20), chromium nitride (Cr_2N), and nitrogenized ferromanganese (Mn87H6) were employed as nitrogen source during the synthesis. In order to investigate how the method of nitrogen introduction during MA affects the nitrogen content and distribution in the alloy, six compositions were examined: 1) Fe–Cr–Ni–Mn–Mo – mechanical alloying in the nitrogen atmosphere; 2) Fe–Cr–Ni–FeMnN–Mo – incorporating manganese in the form of nitrogenized ferromanganese; 3) Fe– Cr_2N –Ni–Mn–Mo – introducing chromium in the form of chromium nitride; 4) Fe–FeCrN–Ni–Mn–Mo – adding chromium in the form of nitrogenized ferrochromium; 5) Fe–(0.5Cr–0.5 Cr_2N)–Ni–Mn–Mo and Fe–(0.5Cr–0.5FeCrN)–Ni–Mn–Mo – incorporating 50 % of the total chromium content in the form of chromium nitride or nitrogenized ferrochrome.

The calculation was conducted utilizing the CALPHAD method through ThermoCalc software for thermodynamic analysis employing the TCHEA4 data package.

Experimental investigations regarding powders plasma spheroidization were carried out using the TekSphero 15 unit (Tekna Plasma Systems Inc., Canada). This unit is equipped with a high-frequency generator reaching a maximum output of 15 kW, operating within a frequency range of 2 to 4 MHz. The experiments were conducted on compositions including Fe–(0.5Cr–0.5 Cr_2N)–Ni–Mn–Mo, Fe– Cr_2N –Ni–Mn–Mo, Fe–(0.5Cr–0.5FeCrN)–Ni–Mn–Mo and Fe–FeCrN–Ni–Mn–Mo within both argon-hydrogen and argon-nitrogen plasma environments.

For studying powder morphology, the SEM Tescan Mira 3 scanning electron microscope (Tescan, Czech Republic) was utilized alongside the X-Flash 6/10 fluorescence detector (Bruker, USA), while the Leica DMI 5000 optical microscope (Leica Microsystems, Germany) aided in obtaining cross-sectional images to assess chemical makeup. The carbon content analysis was conducted using the absorption method via the CS-230 analyzer (LECO, USA, ISO 9556-1989). Determination of oxygen and nitrogen content was carried out by the reducing fusion method in an inert carrier flow (helium) using the TC-500 analyzer (LECO, USA, ISO 17053-2005 and ISO 15351-1999). The particle size distribution analysis of the acquired powder (ISO 8130-13) was performed using the Analysette 22 laser diffractometer (Fritsch GmbH, Germany). X-ray diffraction analysis was conducted using the Bruker D8

Advance X-ray diffractometer (USA) with CuK_α radiation (1.5406 \AA) within the range $2\theta = 30 \div 100^\circ$.

The samples were produced from nitrogen-containing steel powders using the SLM technology within a nitrogen atmosphere, employing the SLM280HL selective laser melting system (SLM Solutions GmbH, Lübeck, Germany). This system is equipped with the YLR laser featuring a wavelength of 1070 nm and focal length of $\sim 80 \text{ }\mu\text{m}$.

Nitrogen-containing steel powders were compacted using the SLM technique. The experiments were conducted on compositions including $\text{Fe}-(0.5\text{Cr}-0.5\text{Cr}_2\text{N})-\text{Ni}-\text{Mn}-\text{Mo}$, $\text{Fe}-\text{Cr}_2\text{N}-\text{Ni}-\text{Mn}-\text{Mo}$, $\text{Fe}-(0.5\text{Cr}-0.5\text{FeCrN})-\text{Ni}-\text{Mn}-\text{Mo}$ and $\text{Fe}-\text{FeCrN}-\text{Ni}-\text{Mn}-\text{Mo}$, synthesized in an argon-hydrogen plasma, influenced by oxygen content within the produced powder. To examine the influence of SLM parameters on the relative density and chemical composition of the resulting alloys, cubic samples with a side length of 10 mm were manufactured. This was achieved by varying laser power, scanning speed, and energy density. The powder layer applied was 0.05 mm thick, and the laser pass spacing was set at 0.12 mm . The specific SLM parameters utilized in these experiments are detailed in Table 1.

Results and discussion

The phase diagram calculation for the $\text{Fe}-16\text{Cr}-2.2\text{Ni}-0.6\text{Mn}-1.1\text{Mo}-0.04\text{C}-\text{N}$ alloy, performed using the ThermoCalc software package for thermodynamic analysis, revealed that the nitrogen concentration limit during crystallization is 0.2 wt. \% . When this limit is surpassed, nitrogen is emitted into the gas phase, potentially leading to the formation of bubbles and pores during crystallization. Throughout solidification, the composition of the liquid phase and the evolving solid phases continuously alter with changes in temperature and the amount of the liquid phase. Consequently, the solubility of nitrogen in δ -ferrite within the tempera-

ture range of $1470\text{--}1750 \text{ K}$ does not exceed 0.07 wt. \% , while in austenite, it reaches 0.6 wt. \% .

It has been observed that during the initial stages of MA, the dissolution of alloying elements in all investigated systems follows a general pattern. Due to significant plastic deformation, the particles from the initial powder undergo flattening and subsequent welding, resulting in the formation of a composite structure. Following a duration of MA for $\tau_{\text{MA}} = 5 \text{ h}$, the composite particles exhibit a characteristic layered structure comprising various combinations of the initial components.

With a prolonged duration of MA, the primary processes involve the homogenization of the composition concerning chemical makeup and the interaction between the initial components aimed at reducing the system's free energy. Analysis of the acquired diffractograms revealed that Ni is the initial alloying element to dissolve into the iron lattice (atomic radius $r_a = 124 \text{ pm}$), followed by Mn ($r_a = 127 \text{ pm}$), Cr ($r_a = 130 \text{ pm}$), and Mo ($r_a = 139 \text{ pm}$). This sequence is attributed to Ni, Mn, and Cr alloying elements forming substitutional solid solutions with iron, whereby the atomic radius of nickel is closest to that of iron ($r_a = 126 \text{ pm}$), followed by manganese, chromium, and molybdenum, respectively. The dissolution of alloying elements leads to a modification of the α -Fe lattice parameter, ranging from 0.2866 to 0.2887 nm , contingent upon the system. Considering the proportions of the components, it is presumable that diffusion predominantly occurs along the crystal lattice defects during the MA process. In both the initial $\text{Fe}-16\text{Cr}-2.2\text{Ni}-0.6\text{Mn}-1.1\text{Mo}$ composition and the one utilizing nitrogenized ferromanganese as the nitrogen source, the alloying elements exhibit nearly uniform distribution throughout the powder volume. They correspond to the chemical composition of the initial mixture after $\tau_{\text{MA}} = 10 \text{ h}$ (Fig. 1, *a*). However, the dissolution of molybdenum is considerably impeded due to its atomic radius being significantly larger than that of the other composition elements. The MA process in these systems is similar owing to the fact that nitrogenized ferromanganese is primarily composed of manganese nitride – a compound easily degraded – with inclusions of iron and a small quantity of ferromanganese from the initial charge.

In systems where chromium nitride (Cr_2N) and nitrogenized ferrochrome (according to XRD results – $80 \text{ vol. \% CrN} + 20 \text{ vol. \% Cr}_2\text{N}$) were utilized as nitrogen sources, the dissolution behavior of alloying elements differed from that in the initial composition. Following $\tau_{\text{MA}} = 10 \text{ h}$, alloying elements exhibited heterogeneous distribution across the volume. Upon reaching $\tau_{\text{MA}} = 15 \text{ h}$, chromium continued to remain non-uniformly distributed, residing inside the particles

Table 1. SLM parameters for printing mode testing

Таблица 1. Параметры СЛП при отработке режимов печати

No.	Laser power, W	Scanning rate, mm/s	$E, \text{ J/mm}^3$
1	240	650	61.54
2	300	800	62.50
3	300	650	76.92
4	360	650	92.31
5	300	500	100.00
6	300	650	115.38

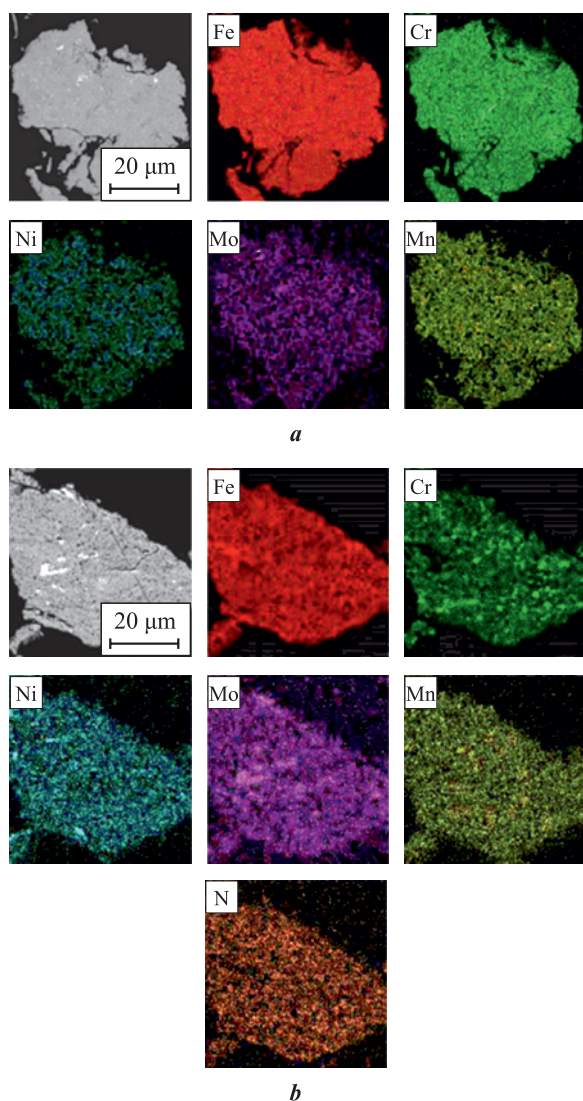


Fig. 1. Component distribution of the Fe-16Cr-2.2Ni-0.6Mn-1.1Mo composition after MA

a – without nitrogen, $\tau_{MA} = 10$ h
b – with nitrogenized ferrochromium, $\tau_{MA} = 15$ h

Рис. 1. Распределение компонентов композиции Fe-16Cr-2,2Ni-0,6Mn-1,1Mo после МЛ

a – без азота, $\tau_{МЛ} = 10$ ч
b – с азотированным феррохромом (ФХ20), $\tau_{МЛ} = 15$ ч

in the form of submicron-sized inclusions evenly dispersed throughout the volume (Fig. 1, *b*). This pattern emerged because chromium was introduced in the form of chromium nitride – a relatively stable chemical compound – not in elemental powder form. Evidently, the energy imparted during the MA process might be insufficient for its breakdown and subsequent dissolution. Upon joint analysis of XRD results and the distribution of alloying elements within particle volumes, it is evident that the decline in Cr_2N peaks is likely attributed to its disintegration and distribution across the volume, rather than its dissolution into the iron lattice (Fig. 2). According to XRD results, a portion of Cr_2N remains

undissolved even after 15 h of mechanical alloying. However, when materials such as chromium nitride or nitrogenized ferrochrome are incorporated at 50 % of the total chromium content, they demonstrate almost complete dissolution into the iron lattice, with only sporadic submicron-sized inclusions observed. This change in solubility may be attributed to the presence of pure chromium, which, due to its high affinity for nitrogen, attracts a portion of the nitrogen from the nitride, expediting its decomposition and facilitating nitrogen diffusion into the lattice.

The nitrogen content analysis in powder samples revealed that throughout the MA process, up to 2.5 wt. % nitrogen can be introduced into the Fe-16Cr-2.2Ni-0.6Mn-1.1Mo alloy, while the equilibrium content remains at 0.1 wt. % (Table 2). The samples employing nitrogenized ferrochrome or chromium nitride as the nitrogen source exhibited the highest nitrogen proportions. With this method of introduction, the nitrogen assimilation rate reached approximately 90 %. According to XRD and SEM results, a major portion of the nitrogen is dissolved within the Fe lattice. However, some nitrogen remains in nitrides, uniformly dispersed throughout the particle volume in the form of submicron-sized inclusions.

The analysis of the particle size distribution in the obtained powders indicates a correlation between higher nitrogen content in the alloy and an increased presence of powder particles smaller than 45 μm . This reduction in particle size is attributed to undissolved submicron nitride inclusions, inducing significant distortions within the crystal lattice and acting as stress concentrators. Under intensive mechanical forces

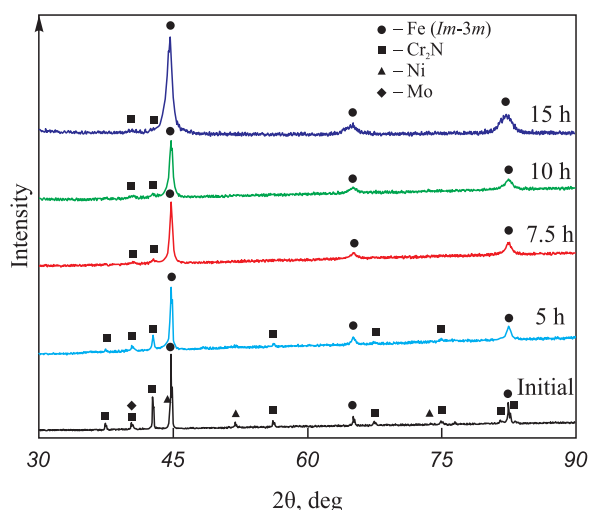


Fig. 2. Evolution of phase constitution with MA duration in Fe- Cr_2N -Ni-Mn-Mo composition

Рис. 2. Изменение фазового состава в зависимости от продолжительности МЛ композиции Fe- Cr_2N -Ni-Mn-Mo

Table 2. Chemical composition of MA-powder for Fe–16Cr–2.2Ni–0.6Mn–1.1Mo alloy

Таблица 2. Химический состав МЛ-порошка сплава Fe–16Cr–2,2Ni–0,6Mn–1,1Mo

Composition	Element content, wt. %						
	Fe	Cr	Ni	Mn	Mo	N	C
Fe–Cr–Ni–Mn–Mo	Basic	16.28	2.10	0.64	1.24	0.02	0.05
Fe–Cr–Ni–FeMnN–Mo	Basic	15.63	2.44	0.83	1.05	0.04	0.19
Fe–Cr ₂ N–Ni–Mn–Mo	Basic	15.92	2.26	0.59	1.29	1.90	0.15
Fe–FeCrN–Ni–Mn–Mo	Basic	15.59	2.37	0.65	1.13	2.48	0.28
Fe–(0.5Cr–0.5Cr ₂ N)–Ni–Mn–Mo	Basic	16.15	2.11	0.82	1.11	1.06	0.14
Fe–(0.5Cr–0.5FeCrN)–Ni–Mn–Mo	Basic	16.23	2.35	0.69	1.02	1.32	0.22

during the MA process, the existence of such stress concentrators tends to prompt crack formation, subsequently leading to material disintegration.

Several research studies [42–44] have highlighted that spherical powders of nitrogen-containing alloy Fe–16Cr–2.2Ni–0.6Mn–1.1Mo with a high degree of sphericity can be produced using thermal argon-hydrogen and argon-nitrogen plasma generated in a high-frequency plasmatron (Fig. 3). Investigation into powder particle morphology indicated that the proportion of spheroidized particles in the resulting powders ranges between 70–96 %. It was observed that, at the same powder feed rate, the occurrence of non-spherical particles after spheroidization in argon-nitrogen plasma is higher due to differing physical and chemical properties of the plasma-forming gas mixtures. Hydrogen dissociates by 90 % at $T = 4700$ K, while nitrogen does so at $T = 9000$ K, significantly affecting the plasma's heat content (enthalpy). To achieve powders with an equivalent proportion of spheroidized particles, the powder feed rate in argon-nitrogen plasma needs to be reduced by 10–15 %.

The analysis of SEM images and particle size distribution in the obtained powders has revealed distinct characteristics. Powders with low nitrogen content (Fe–Cr–Ni–Mn–Mo, Fe–Cr–Ni–FeMnN–Mo compositions) exhibited a differential curve in the particle size distribution after plasma spheroidization. The peak of this curve lies within the range of 30 to 125 μm , indicating a slight shift towards smaller sizes compared to the initial material (which ranged from 45 to 125 μm). Conversely, in powders with high nitrogen content, a considerable proportion (about 30–50 %) of particles emerged with sizes below 30 μm , despite the initial powder size range being 45 to 125 μm . These variations suggest the presence of elevated mechanical stresses and microcracks within the powder particles, likely a consequence of the intense mechanical impact during the MA process. The initial plasma temperature significantly surpasses the material's boiling point, not merely its melting point. Consequently, the powder particles experience rapid melting. During this swift heating and melting process, nitrogen might be swiftly released from the solution, transforming into the gaseous phase at a high rate. This phenomenon contributes to the wedging

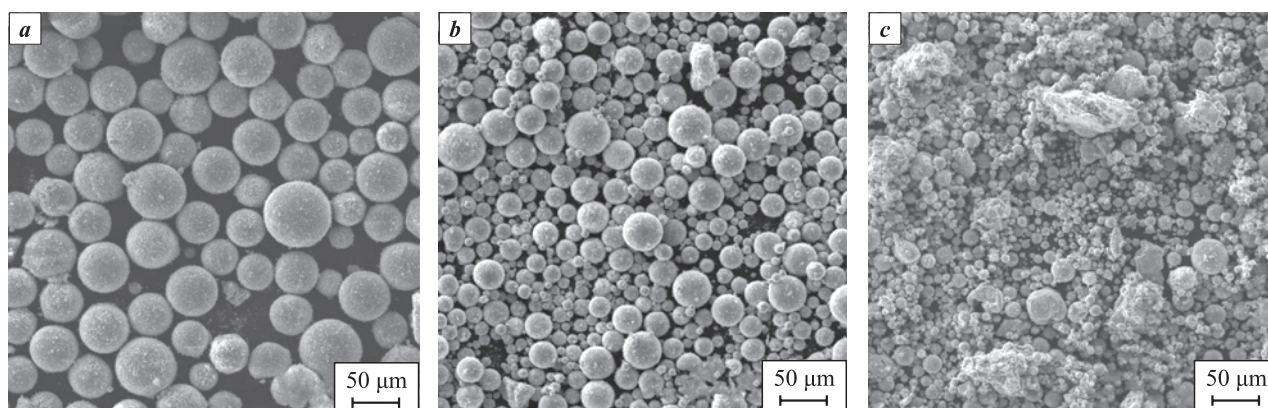


Fig. 3. Powder morphology after plasma spheroidization

a – Fe–Cr–Ni–Mn–Mo; *b* – Fe–(0.5Cr–0.5Cr₂N)–Ni–Mn–Mo; *c* – Fe–Cr₂N–Ni–Mn–Mo

Рис. 3. Морфология порошка после плазменной сфероидизации

a – Fe–Cr–Ni–Mn–Mo; *b* – Fe–(0,5Cr–0,5Cr₂N)–Ni–Mn–Mo; *c* – Fe–Cr₂N–Ni–Mn–Mo

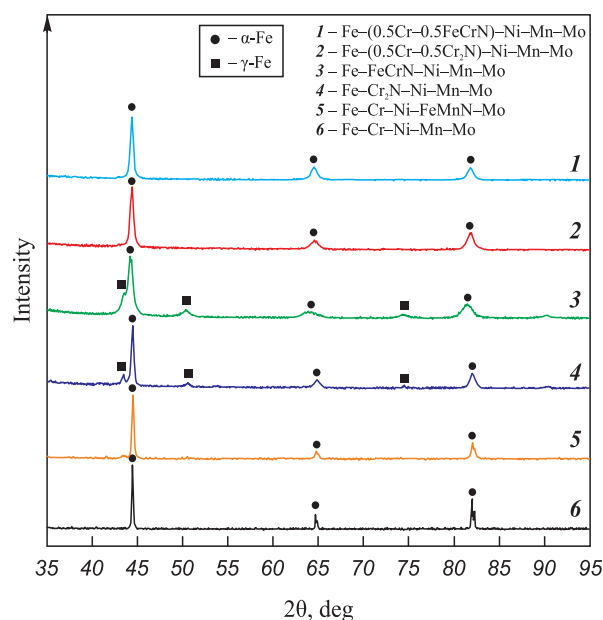


Fig. 4. Phase composition of Fe–Cr–Ni–Mn–Mo alloy powders after spheroidization in argon-hydrogen plasma

Рис. 4. Фазовый состав порошков сплава Fe–Cr–Ni–Mn–Mo после сфероидизации в аргонородородной плазме

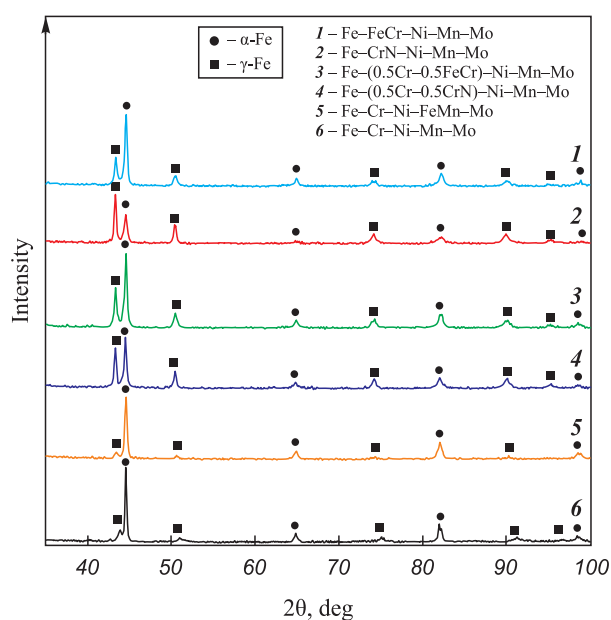


Fig. 5. Phase composition of Fe–Cr–Ni–Mn–Mo alloy powders after spheroidization in argon-nitrogen plasma

Рис. 5. Фазовый состав порошков сплава Fe–Cr–Ni–Mn–Mo после сфероидизации в аргонноазотной плазме

of microcracks and the destruction of particles before melting occurs, or during the intensive boiling and disintegration of already-melted particles. Some powders were found to contain individual hollow spheres, primarily exhibiting a cracked shell structure.

The X-ray phase analysis conducted on the powders post-spheroidization revealed the existence of α - and γ -Fe peaks (Fig. 4, 5). Nitrogen, being an element conducive to austenite formation, results in a marginal increase in the proportion of γ -Fe as the nitrogen content

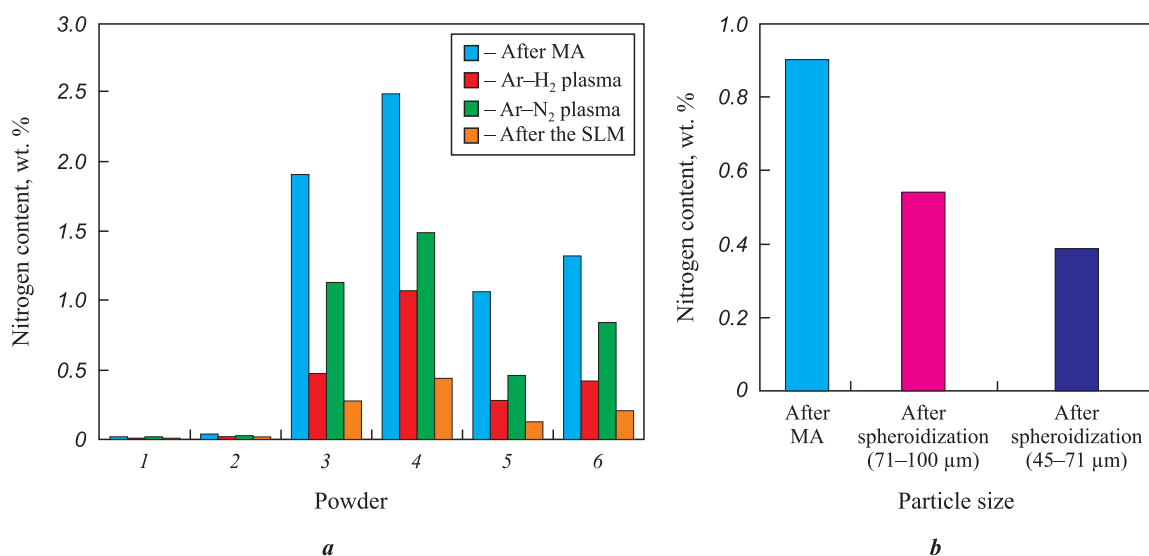


Fig. 6. Nitrogen content in powders post plasma flow treatment (a) and particle size-dependent nitrogen content variation (b)

1 – Fe–Cr–Ni–Mn–Mo; 2 – Fe–Cr–Ni–FeMnN–Mo; 3 – Fe–Cr₂N–Ni–Mn–Mo; 4 – Fe–FeCrN–Ni–Mn–Mo;
5 – Fe–(0.5Cr–0.5Cr₂N)–Ni–Mn–Mo; 6 – Fe–(0.5Cr–0.5FeCrN)–Ni–Mn–Mo

Рис. 6. Содержание азота в порошках после обработки в потоке плазмы (a) и зависимость содержания азота от размера частиц (b)

1 – Fe–Cr–Ni–Mn–Mo; 2 – Fe–Cr–Ni–FeMnN–Mo; 3 – Fe–Cr₂N–Ni–Mn–Mo; 4 – Fe–FeCrN–Ni–Mn–Mo;
5 – Fe–(0.5Cr–0.5Cr₂N)–Ni–Mn–Mo; 6 – Fe–(0.5Cr–0.5FeCrN)–Ni–Mn–Mo

in the alloy elevates. The phase composition of the powders subsequent to plasma spheroidization aligns with the results derived from the calculated state diagrams, indicating that the powders are in a quenched state.

The investigation revealed that a portion of nitrogen is lost from the alloy during spheroidization in plasma. Post-spheroidization, in argon-hydrogen plasma, the nitrogen content ranges between 0.01 to 1.0 wt. %, showcasing a decrease by 50–75 % (Fig. 6, *a*). Conversely, in argon-nitrogen plasma, the nitrogen content experiences a maximum reduction of 40 %. The use of argon-nitrogen plasma leads to the chamber atmosphere becoming saturated with molecular (N_2) and atomic (N^+) nitrogen ions. This occurrence arises from the excitation of electronic states within molecules by oscillating electrons in the flow of high-temperature argon plasma, followed by the subsequent decomposition of excited molecules. Consequently, this saturation contributes to an increased limit concentration of nitrogen within the melt during crystallization. Additionally, it slows down the release of nitrogen from the melt and aids in plasma-chemical nitriding processes. The variance in nitrogen content concerning the fractional composition of the powder mixture can be attributed to diffusion processes. Specifically, it involves the differential distance of nitrogen diffusion from the powder particle to its surface during spheroidization when the powder transforms into metal droplets. Furthermore, differences in the temperature of molten metal droplets play a role in this variation. Therefore, particles with smaller diameters tend to exhibit a lower mass fraction of nitrogen compared to particles with larger diameters. Regarding residual nitrogen amounts, the investigation found 0.54 wt. % in the powder fraction of 71–100 μm and 0.39 wt. % in the powder ranging from 45–71 μm . This is in contrast to the initial alloy's nitrogen content, which was approximately ~0.9 wt. % (Fig. 6, *b*).

In the process of spheroidization, when hydrogen is introduced into the plasma-forming gas, oxides are reduced, resulting in a decrease in the oxygen content to levels lower than 0.1 wt. % across all compositions. Conversely, during spheroidization in argon-nitrogen plasma, the reduction in oxygen content occurs primarily due to the evaporation of the oxide phase from the surface of molten particles, followed by subsequent condensation into submicron particles. Chemical analysis revealed that the oxygen content in the powders produced via spheroidization in argon-nitrogen plasma ranges between 0.2 and 0.3 wt. %.

The testing of the obtained powders in the SLM unit resulted in the formation of compact alloys showcasing a minimum porosity of 0.8 % (as depicted in Fig. 7). Notably, an increase in the initial powder's

nitrogen content correlates with a rise in the minimum alloy porosity, reaching up to 11.5 %. During the SLM process, the nitrogen content in the alloy ranges from 0.13 to 0.44 wt. %, exceeding the nitrogen concentration limit during crystallization by twofold. This excess in nitrogen concentration prompts a challenge in steel solidification, where nitrogen release occurs into the gas phase, leading to the formation of nitrogen bubbles and subsequent porosity within the material. Throughout solidification, there's a continual alteration in the composition of the liquid and solid phases, contingent upon variations in temperature and the quantity of the liquid phase. Moreover, the local solubility of nitrogen in the residual liquid phase experiences changes, depending on the type of crystallization (austenitic, ferritic, or mixed) and the proportion of phase quantities. Ensuring compliance with a specific condition throughout the entire solidification duration is crucial for obtaining a dense ingot [45]:

$$[N]_{L, T} < [N]_{L, eq, P_{tot}},$$

where $[N]_{L, T}$ is the nitrogen content in the residual liquid at temperature T ; $[N]_{L, eq, P_{tot}}$ is the equilibrium nitrogen content in the liquid metal at the same temperature T and under the total pressure in the system.

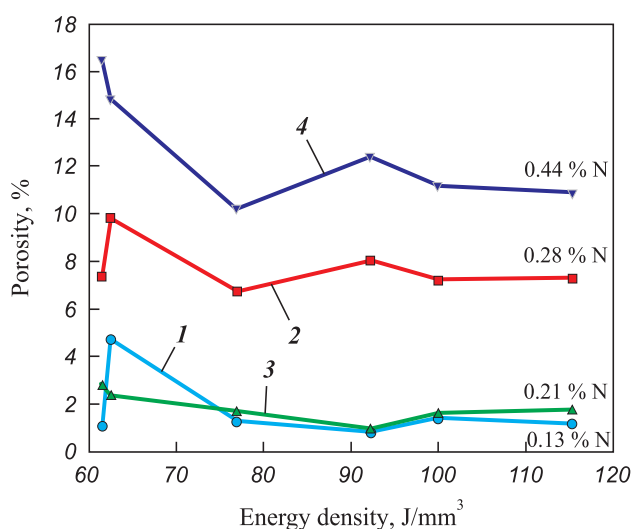


Fig. 7. Relative porosity of alloys fabricated via selective laser melting at various energy density levels

- 1 – Fe-(0.5Cr–0.5Cr₂N)–Ni–Mn–Mo
- 2 – Fe–Cr₂N–Ni–Mn–Mo
- 3 – Fe-(0.5Cr–0.5FeCrN)–Ni–Mn–Mo
- 4 – Fe–FeCrN–Ni–Mn–Mo

Рис. 7. Относительная пористость сплавов, полученных методом селективного лазерного плавления с разной плотностью энергии

- 1 – Fe-(0,5Cr–0,5Cr₂N)–Ni–Mn–Mo
- 2 – Fe–Cr₂N–Ni–Mn–Mo
- 3 – Fe-(0,5Cr–0,5FeCrN)–Ni–Mn–Mo
- 4 – Fe–FeCrN–Ni–Mn–Mo

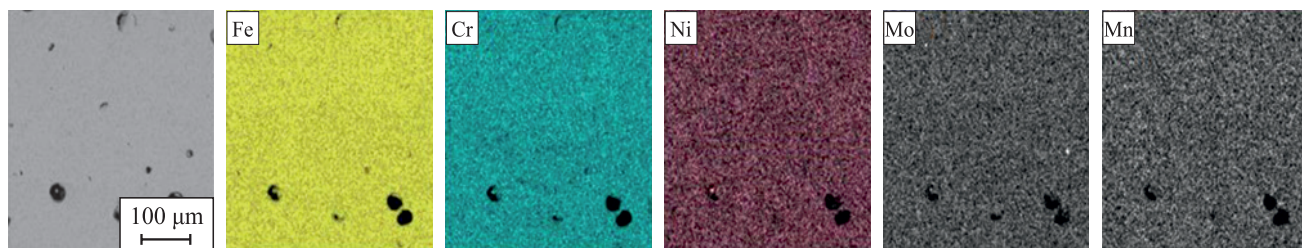


Fig. 8. Component distribution in Fe-FeCrN-Ni-Mn-Mo composition after SLM

Рис. 8. Распределение компонентов в композиции Fe-FeCrN-Ni-Mn-Mo после СЛП

As noted above, the limit concentration of nitrogen during crystallization of the studied alloy does not exceed 0.2 wt. %. The actual nitrogen content in the liquid phase during printing is greater than its equilibrium solubility, the pressure in the chamber being 1 atm, so

nitrogen is released in the gaseous state. It is worth noting that the porosity of alloys obtained from powders in which nitrogenized ferrochrome was used as the source of nitrogen is higher than that of alloys with chromium nitride, which is due to the higher decomposition tem-

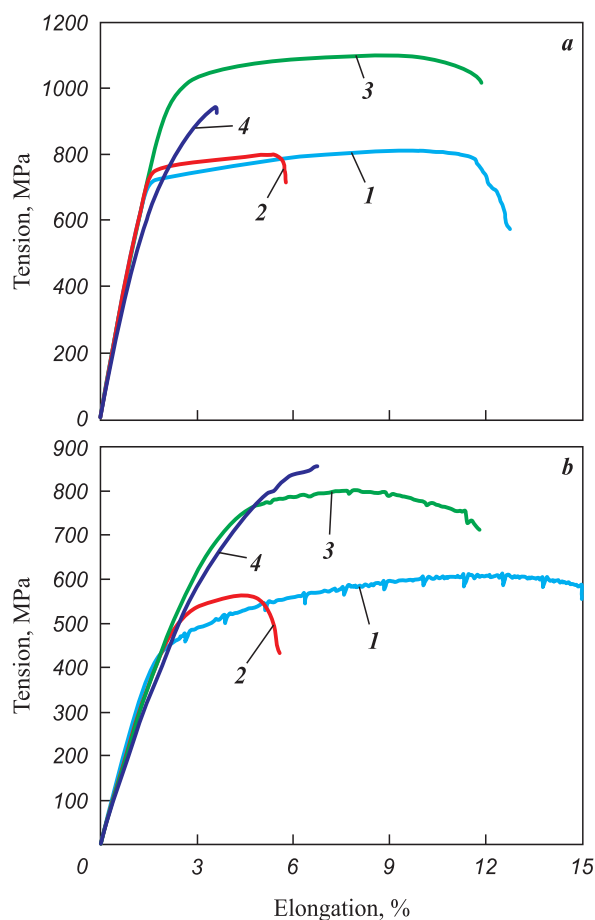


Fig. 9. Stretching diagram of alloys fabricated via SLM method

Test temperature: *a* – 20 °C; *b* – 500 °C

1 – Fe-(0.5Cr-0.5Cr₂N)-Ni-Mn-Mo; 2 – Fe-Cr₂N-Ni-Mn-Mo
3 – Fe-(0.5Cr-0.5FeCrN)-Ni-Mn-Mo; 4 – Fe-FeCrN-Ni-Mn-Mo

Рис. 9. Диаграмма растяжения сплавов, полученных методом СЛП

Температура испытаний: *a* – 20 °C; *b* – 500 °C

1 – Fe-(0.5Cr-0.5Cr₂N)-Ni-Mn-Mo; 2 – Fe-Cr₂N-Ni-Mn-Mo
3 – Fe-(0.5Cr-0.5FeCrN)-Ni-Mn-Mo; 4 – Fe-FeCrN-Ni-Mn-Mo

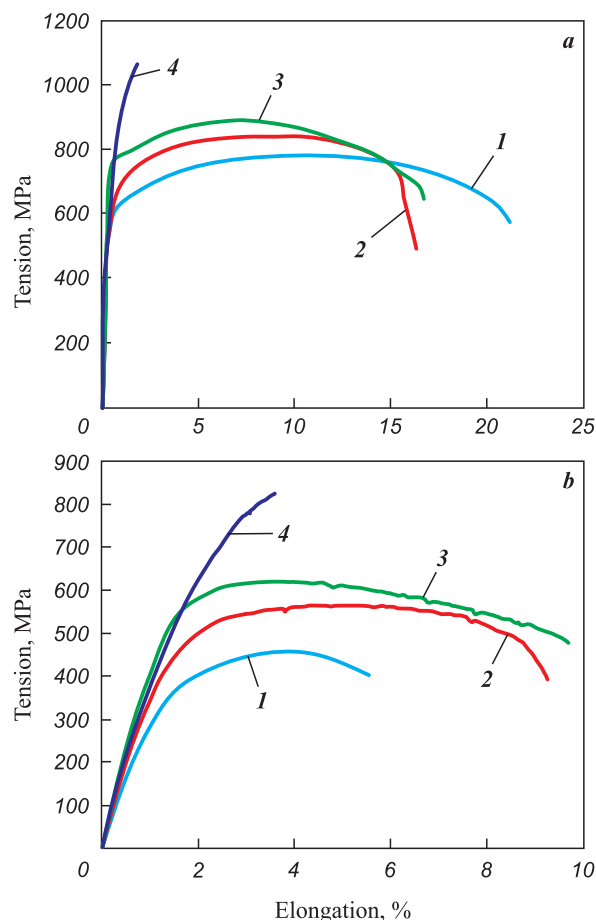


Fig. 10. Stretching diagram of alloys fabricated via SLM method followed by HIP

Test temperature: *a* – 20 °C; *b* – 500 °C

1 – Fe-(0.5Cr-0.5Cr₂N)-Ni-Mn-Mo; 2 – Fe-Cr₂N-Ni-Mn-Mo
3 – Fe-(0.5Cr-0.5FeCrN)-Ni-Mn-Mo; 4 – Fe-FeCrN-Ni-Mn-Mo

Рис. 10. Диаграмма растяжения сплавов, полученных методом СЛП с последующим ГИП

Температура испытаний: *a* – 20 °C; *b* – 500 °C

1 – Fe-(0.5Cr-0.5Cr₂N)-Ni-Mn-Mo; 2 – Fe-Cr₂N-Ni-Mn-Mo
3 – Fe-(0.5Cr-0.5FeCrN)-Ni-Mn-Mo; 4 – Fe-FeCrN-Ni-Mn-Mo

Table 3. Mechanical properties of alloys fabricated via SLM method
Таблица 3. Механические свойства сплавов, полученных методом СЛП

Composition	SLM						SLM and HIP					
	20 °C			500 °C			20 °C			500 °C		
	$\sigma_{0.2}$, MPa	σ_u , MPa	δ , %	$\sigma_{0.2}$, MPa	σ_u , MPa	δ , %	$\sigma_{0.2}$, MPa	σ_u , MPa	δ , %	$\sigma_{0.2}$, MPa	σ_u , MPa	δ , %
Fe–Cr ₂ N–Ni–Mn–Mo	730	780	5.5	480	560	5	620	840	16.0	400	560	8.2
Fe–FeCrN–Ni–Mn–Mo	–	980	–	600	820	4	800	1070	1.2	600	830	1.4
Fe–(0.5Cr–0.5Cr ₂ N)–Ni–Mn–Mo	700	790	12.0	430	610	10	610	780	21.0	370	460	4.0
Fe–(0.5Cr–0.5FeCrN)–Ni–Mn–Mo	960	1100	10.5	560	800	9	770	890	16.0	530	620	8.5
15X16H2AM (According to TS14-1-1431-75)	740	935	14.0	540	640	–	740	935	14.0	540	640	–

perature of the latter. Further investigation into the distribution of elements revealed that the alloying elements exhibit an even distribution across the cross-sections of the alloys (Fig. 8).

The obtained alloys underwent heat treatment following this procedure: quenching from a temperature of 1040 ± 10 °C in oil, followed by tempering within the range of 640 to 680 °C for 2 h. Mechanical tests conducted at room temperature and at 500 °C revealed (Fig. 9 and Table 3) that the alloys produced via the SLM technology did not meet the specifications' requirements for the Fe16Cr2.2Ni0.6Mn1.1Mo0.1N alloy due to excessive porosity, resulting in inadequate relative elongation. In order to mitigate the porosity issue, the alloys underwent hot isostatic pressing (HIP) at 1160 °C and a pressure of 150 MPa for 3 h. Following HIP treatment, the porosity in the alloys was successfully reduced to not exceeding 0.2 %, consequently enhancing the material's ductility at room temperature (Fig. 10, Table 3).

The heat treatment applied to the SLM alloys followed the standard mode specified in the TS for Fe16Cr2.2Ni0.6Mn1.1Mo0.1N steel. However, due to variations in carbon content between the synthesized alloy and the Fe16Cr2.2Ni0.6Mn1.1Mo0.1N steel composition (TS14-1-1431-75), the heat treatment methods as outlined in TS do not yield the most optimal properties for the synthesized alloy. Consequently, adjustments in the heat treatment modes are required, which will be the focus of future research.

Conclusion

The study revealed that during the initial stages of the MA process, regardless of the method of nitrogen introduction, the dissolution of alloying elements in all investigated systems follows a general pattern, forming a layered composite structure. When nitro-

gen is introduced as chromium nitride (Cr₂N), it is not fully dissolved in the iron lattice; instead, it distributes evenly throughout the volume as submicron inclusions. The stability of chromium nitride as a chemical compound might prevent its complete decomposition and dissolution due to the insufficient energy flow during the MA process.

By employing various nitrogen-containing initial components in the MA process, nitrogen up to 2.5 wt. % can be introduced, whereas the crystallization limit concentration remains ≤ 0.2 wt. %. Consequently, the degree of nitrogen assimilation reaches approximately 90 %. The increase in nitrogen content in the alloy correlates with a higher proportion of powder particles ≤ 45 μ m in size. This is attributed to significant distortions in the crystal lattice caused by submicron nitride inclusions, resulting in crack formation and subsequent material disintegration.

During spheroidization in argon-hydrogen plasma, there is a reduction in nitrogen content by 50–75 % from its initial levels, while spheroidization in argon-nitrogen plasma leads to a decrease in nitrogen content by no more than 40 %. Synthesis of powders with a spherical shape and nitrogen content up to 1.2 wt. % was demonstrated, depending on the method of nitrogen introduction in the MA process and the composition of the plasma-forming gas.

The investigation delved into the impact of SLM process parameters on nitrogen content in alloys, their porosity, and mechanical properties. As the nitrogen amount in the alloy increases, the minimum porosity escalates to 11.5 %. Nitrogen content in the alloy obtained by SLM ranges from 0.13 to 0.44 wt. %, which surpasses the nitrogen concentration limit during crystallization twice. Mechanical tests affirmed that the alloys produced via selective laser melting exhibit comparable characteristics to those obtained using traditional metallurgical methods.

References / Список литературы

1. Svyazhin A.G., Kaputkina L.M. Nitrogen steels and high nitrogen steels. Industrial technologies and properties. *Izvestiya. Ferrous Metallurgy*. 2019;62(3):173–187. (In Russ.). <https://doi.org/10.17073/0368-0797-2019-3-173-187>
 Свяжин А.Г., Капуткина Л.М. Азотистые и высокоазотистые стали. Промышленные технологии и свойства. *Известия высших учебных заведений. Черная металлургия*. 2019;62(3):173–187. <https://doi.org/10.17073/0368-0797-2019-3-173-187>
2. Stein G., Hucklenbroich I. Manufacturing and applications of high nitrogen steels. *Materials and Manufacturing Processes*. 2004;19(1):7–17. <https://doi.org/10.1081/AMP-120027494>
3. Foct J., Domain C., Becquart C.S. High nitrogen steel and interstitial alloying. *Material Science Forum*. 2003; 426–432:161–170.
4. Qi-zeng L. Rapidly growing stainless steel industry in China. *Ironmaking Steelmaking*. 2006;10(1):112.
5. Speidel M.O. Nitrogen containing austenitic stainless steels. *Materialwissenschaft und Werkstofftechnik*. 2006; 37(10):875–880. <https://doi.org/10.1002/mawe.200600068>
6. Sun X., Ren J., Wang Y., Zhao D., Wang S., Xiong X., Rao J.H. Nitriding behaviour and microstructure of high-nitrogen stainless steel during selective laser melting. *Materials*. 2023;16(6):2505. <https://doi.org/10.3390/ma16062505>
7. Zheng Z., Wang L., Jia M., Cheng L., Yan B. Microstructure and mechanical properties of stainless steel/calcium silicate composites manufactured by selective laser melting. *Materials Science and Engineering: C*. 2017;71:1099–1105. <https://doi.org/10.1016/j.msec.2016.11.032>
8. Cheng B. Ambient pressure fabrication of Ni-free high nitrogen austenitic stainless steel using laser powder bed fusion method. *Additive Manufacturing*. 2022;55:102810. <https://doi.org/10.1016/j.addma.2022.102810>
9. Boes J., Röttger A., Theisen W., Cui C., Uhlenwinkel V., Schulz A., Walther F. Gas atomization and laser additive manufacturing of nitrogen-alloyed martensitic stainless steel. *Additive Manufacturing*. 2020;34:101379. <https://doi.org/10.1016/j.addma.2020.101379>
10. Yang K., Wang Z.D., Chen M.Z., Lan H.F., Sun G.F., Ni Z.H. Effect of pulse frequency on the morphology, microstructure, and corrosion resistance of high-nitrogen steel prepared by laser directed energy deposition. *Surface Coatings Technologies*. 2021;421:127450. <https://doi.org/10.1016/j.surfcoat.2021.127450>
11. Springer H., Baron C., Szczepaniak A., Jäggle E.A., Wilms M.B., Weisheit A., Raabe D. Efficient additive manufacturing production of oxide- and nitride-dispersion-strengthened materials through atmospheric reactions in liquid metal deposition. *Materials and Design*. 2016;111:60–69. <https://doi.org/10.1016/j.matdes.2016.08.084>
12. Pauzon C., Hryha E., Forêt P., Nyborg L. Effect of argon and nitrogen atmospheres on the properties of stainless steel 316 L parts produced by laser-powder bed fusion. *Material and Design*. 2019;179:107873. <https://doi.org/10.1016/j.matdes.2019.107873>
13. Boes J., Röttger A., Theisen W. Microstructure and properties of high-strength C + N austenitic stainless steel processed by laser powder bed fusion. *Additive Manufacturing*. 2020;32:101081. <https://doi.org/10.1016/j.addma.2020.101081>
14. Becker L., Röttger A., Boes J., Weber S., Theisen W. Processing of a newly developed nitrogen-alloyed ferritic-austenitic stainless steel by laser powder bed fusion – microstructure and properties. *Additive Manufacturing*. 2021;46:102185. <https://doi.org/10.1016/j.addma.2021.102185>
15. Arabi-Hashemi A., Maeder X., Figi R., Schreiner C., Griffiths S., Leinenbach C. 3D magnetic patterning in additive manufacturing via site-specific in-situ alloy modification. *Applied Materials Today*. 2020;18:100512. <https://doi.org/10.1016/j.apmt.2019.100512>
16. Zhang X., Zhou Q., Wang K., Peng Y., Ding J., Kong J., Williams S. Study on microstructure and tensile properties of high nitrogen Cr–Mn steel processed by CMT wire and arc additive manufacturing. *Materials and Design*. 2019;166:107611. <https://doi.org/10.1016/j.matdes.2019.107611>
17. Zhang X., Zhou Q., Wang K., Peng Y., Ding J., Kong J., Williams S. Precipitation characteristics and tensile properties of high-nitrogen chromium-manganese steel fabricated by wire and arc additive manufacturing with isothermal post-heat treatment. *Material and Design*. 2023;225: 111536. <https://doi.org/10.1016/j.matdes.2022.111536>
18. A Hosseini V., Höglström M., Hurtig K., Valiente Bermejo M.A., Stridh L.-E., Karlsson L. Wire-arc additive manufacturing of a duplex stainless steel: thermal cycle analysis and microstructure characterization. *Welding in the World*. 2019;63(4):975–987. <https://doi.org/10.1007/s40194-019-00735-y>
19. Wu T., Liu J., Wang K., Wang L., Zhang X. Microstructure and mechanical properties of wire-powder hybrid additive manufacturing for high nitrogen steel. *Journal of Manufacturing Processes*. 2021;70:248–258. <https://doi.org/10.1016/j.jmapro.2021.08.029>
20. Astafurov S., Astafurova E., Reunova K., Melnikov E., Panchenko M., Moskvina V., Kolubaev E. Electron-beam additive manufacturing of high-nitrogen steel: Microstructure and tensile properties. *Material Science and Engineering: A*. 2021;826:141951. <https://doi.org/10.1016/j.msea.2021.141951>
21. Reunova K.A., Astafurova E.G., Astafurov S.V., Melnikov E.V., Panchenko M.Y., Moskvina V.A., Kolubaev E.A. Microstructure and phase composition of vanadium-alloyed high-nitrogen steel fabricated by additive manufacturing. *AIP Conference Proceedings*. 2020;2310(1):020276. <https://doi.org/10.1063/5.0034265>
22. Panin V.E., Narkevich N.A., Durakov V.G., Shulepov I.A. Control of the structure and wear resistance of a carbon-nitrogen austenitic steel coating produced by electron beam cladding. *Physical Mesomechanics*. 2021;24(1):53–60. <https://doi.org/10.1134/S1029959921010082>
23. Cui C., Uhlenwinkel V., Schulz A., Zoch H.-W. Austenitic stainless steel powders with increased nitrogen content for

- laser additive manufacturing. *Metals*. 2019;10(1):61.
<https://doi.org/10.3390/met10010061>
24. Kuznetsov P.A., Shakirov I.V., Bobyr' V.V., Zhukov A.S., Klimov V.N. Features of melt gas atomization and selective laser melting of high-strength austenitic nitrogen-containing steel powders. *Metal Science and Heat Treatment*. 2020;62(1):76–80.
<https://doi.org/10.1007/s11041-020-00515-2>
25. Ni G., Wang S., Li Q., Zhao D., Song C., Li C. Preparation of Cr17Mn11Mo3N powders by high-pressure gas atomization and the nitrogen increasing mechanism. *Powder Technology*. 2021;385:490–500.
<https://doi.org/10.1016/j.powtec.2021.03.025>
26. Chen D., Daoud H., Scherm F., Klötzer B., Hauack C., Glatzel U. Stainless steel powder produced by a novel arc spray process. *Journal of Materials Research Technology*. 2020;9(4):8314–8322.
<https://doi.org/10.1016/j.jmrt.2020.05.076>
27. Gammal T.E., Abdel-Karim R., Walter M.T., Wosch E., Feldhaus S. High nitrogen steels. High nitrogen steel powder for the production of near net shape parts. *ISIJ International*. 1996;36(7):915–921.
<https://doi.org/10.2355/isijinternational.36.915>
28. Shen H., Zou J., Li Y., Li D., Yu Y., Wang X. Effects of nitrogen on predominant sintering mechanism during the initial stage of high nitrogen nickel-free stainless steel powder. *Journal of Alloys and Compounds*. 2023;945:169230.
<https://doi.org/10.1016/j.jallcom.2023.169230>
29. Boes J., Röttger A., Becker L., Theisen W. Processing of gas-nitrided AISI 316L steel powder by laser powder bed fusion – Microstructure and properties. *Additive Manufacturing*. 2019;30:100836.
<https://doi.org/10.1016/j.addma.2019.100836>
30. Mohammed R., Reddy G.M., Rao K.S. Effect of filler wire composition on microstructure and pitting corrosion of nickel free high nitrogen stainless steel GTA welds. *Transactions of the Indian Institute of Metals*. 2016;69(10):1919–1927.
<https://doi.org/10.1007/s12666-016-0851-6>
31. Gawlik J., Schmidt J., Nowak T., Wójcicki Z., Zagórski A. Nitrogen as an alloying element improving material properties of the high carbon cast steel for ball mill liner plates. *Archives of Civil Mechanical Engineering*. 2017;17(4):926–934.
<https://doi.org/10.1016/j.acme.2017.04.007>
32. Wendler M., Weiß A., Krüger L., Mola J., Franke A., Kovalev A., Wolf S. Effect of manganese on microstructure and mechanical properties of cast high alloyed CrMnNi–N steels. *Advanced Engineering Materials*. 2013;15(7):558–565.
<https://doi.org/10.1002/adem.201200318>
33. Liu Z., Fan C., Chen C., Ming Z., Yang C., Lin S., Wang L. Design and evaluation of nitrogen-rich welding wires for high nitrogen stainless steel. *Journal of Materials Processing Technology*. 2021;288:116885.
<https://doi.org/10.1016/j.jmatprotec.2020.116885>
34. Kikuchi Y., Matsuda F., Okabe T., Ohta M. Nitrogen content of 316L weld metal and its fine particle by means of high-pressure MIG arc welding. *ISIJ International*. 1996;36(7):977–982.
<https://doi.org/10.2355/isijinternational.36.977>
35. Zhao L., Tian Z., Peng Y. Porosity and nitrogen content of weld metal in laser welding of high nitrogen austenitic stainless steel. *ISIJ International*. 2007;47(12):1772–1775.
<https://doi.org/10.2355/isijinternational.47.1772>
36. Qiang W., Wang K. Shielding gas effects on double-sided synchronous autogenous GTA weldability of high nitrogen austenitic stainless steel. *Journal of Materials Processing Technology*. 2017;(250):169–181.
<https://doi.org/10.1016/j.jmatprotec.2017.07.021>
37. Liu Z., Fan C., Ming Z., Chen C., Liu A., Yang C., Wang L. Gas metal arc welding of high nitrogen stainless steel with Ar–N₂–O₂ ternary shielding gas. *Defence Technology*. 2021;17(3):923–931.
<https://doi.org/10.1016/j.dt.2020.05.021>
38. Du Toit M., Pistorius P.C. The influence of oxygen on the nitrogen content of autogenous stainless steel arc welds. *American Welding Society*. 2007;86(8):222S–230S.
39. Yang D., Huang Y., Fan J., Jin M., Peng Y., Wang K. Effect of N₂ content in shielding gas on formation quality and microstructure of high nitrogen austenitic stainless steel fabricated by wire and arc additive manufacturing. *Journal of Manufacturing Process*. 2021;(61)261–269.
<https://doi.org/10.1016/j.jmapro.2020.11.020>
40. Liu Z., Fan C., Chen C., Ming Z., Liu A., Yang C., Wang L. Optimization of the microstructure and mechanical properties of the high nitrogen stainless steel weld by adding nitrides to the molten pool. *Journal of Manufacturing Processes*. 2020;49:355–364.
<https://doi.org/10.1016/j.jmapro.2019.12.017>
41. Du Toit M., Pistorius P.C. Nitrogen control during the autogenous arc welding of stainless steel. Part 2: A kinetic model for nitrogen absorption and desorption. *American Welding Society*. 2003;82(9):231S–237S.
<https://doi.org/10.1007/BF03266398>
42. Razumov N.G., Popovich A.A., Wang Q.S. Thermal plasma spheroidization of high-nitrogen stainless steel powder alloys synthesized by mechanical alloying. *Metals and Materials International*. 2018;24(2):363–370.
<https://doi.org/10.1007/s12540-018-0040-8>
43. Popovich A.A., Razumov N.G. A study of the process of mechanical alloying of iron with austenite-forming elements. *Metal Science and Heat Treatment*. 2015;56(9–10):570–576.
<https://doi.org/10.1007/s11041-015-9801-X>
44. Popovich A.A., Razumov N.G. Dissolution of alloying elements and phase formation in powder materials Fe–18Cr–8Ni–12Mn–xN during mechanical alloying. *Advanced Materials Letters*. 2014;5(12):683–687.
<https://doi.org/10.5185/amlett.2014.6585>
45. Makhmutov T., Razumov N., Kim A., Ganin S., Shamshurin A., Popovich A., Popovich V. Microstructure and mechanical properties of high-nitrogen 16Cr–2Ni–Mn–Mo–xN stainless steel obtained by powder metallurgy techniques. *Materials Today: Proceedings*. 2020; 30(3): 768–772. <https://doi.org/10.1016/j.matpr.2020.01.564>

Information about the Authors




Nikolai E. Ozerskoi – Research Associate of the Research and Educational Center “Additive technologies”, Peter the Great St. Petersburg Polytechnic University (SPbPU)

 **ORCID:** 0000-0002-7371-558X

 **E-mail:** nikolaiozerskoi@yandex.ru

Nikolai G. Razumov – Cand. Sci. (Eng.), Head of the Laboratory “Synthesis of new materials and structures”, SPbPU


 **ORCID:** 0000-0002-7147-6239

 **E-mail:** n.razumov@onti.spbstu.ru

Aleksey O. Silin – Leading Engineer of the Research and Educational Center “Structural and functional materials”, SPbPU


 **E-mail:** silin_ao@spbstu.ru

Evgenii V. Borisov – Cand. Sci. (Eng.), Leading Researcher of the Laboratory “Synthesis of new materials and structures”, SPbPU

 **ORCID:** 0000-0003-2464-6706

 **E-mail:** evgenii.borisov@icloud.com

Anatoly A. Popovich – Dr. Sci. (Eng.), Professor, Director of the Institute of Machinery, Materials and Transport, SPbPU

 **ORCID:** 0000-0002-5974-6654

 **E-mail:** popovicha@mail.ru

Сведения об авторах

Николай Евгеньевич Озерской – научный сотрудник научно-образовательного центра «Аддитивные технологии» Санкт-Петербургского политехнического университета Петра Великого (СПбПУ)

 **ORCID:** 0000-0002-7371-558X

 **E-mail:** nikolaiozerskoi@yandex.ru

Николай Геннадьевич Разумов – к.т.н., заведующий лабораторией «Синтез новых материалов и конструкций» СПбПУ

 **ORCID:** 0000-0002-7147-6239

 **E-mail:** n.razumov@onti.spbstu.ru

Алексей Олегович Силин – ведущий инженер научно-образовательного центра «Конструкционные и функциональные материалы» СПбПУ

 **E-mail:** silin_ao@spbstu.ru

Евгений Владиславович Борисов – к.т.н., ведущий научный сотрудник лаборатории «Синтез новых материалов и конструкций» СПбПУ

 **ORCID:** 0000-0003-2464-6706

 **E-mail:** evgenii.borisov@icloud.com

Анатолий Анатольевич Попович – д.т.н., профессор, директор Института машиностроения, материалов и транспорта СПбПУ

 **ORCID:** 0000-0002-5974-6654

 **E-mail:** popovicha@mail.ru

Contribution of the Authors



N. E. Ozerskoi – conducted experiments, processed obtained results, authored the article, participated in result discussions.

N. G. Razumov – conducted critical literature analysis, contributed to result discussions, drew study conclusions.

A. O. Silin – conducted experiments, participated in result discussions.

E. V. Borisov – planned experiments, fabricated samples, participated in result discussions.

A. A. Popovich – conceptualized the idea, defined the work’s purpose and objectives, participated in result discussions.

Вклад авторов

Н. Е. Озерской – проведение экспериментов, обработка полученных результатов, написание статьи, участие в обсуждении результатов.

Н. Г. Разумов – критический анализ литературы, участие в обсуждении результатов, формирование выводов исследования.

А. О. Силин – проведение экспериментов, участие в обсуждении результатов.

Е. В. Борисов – планирование экспериментов, изготовление образцов, участие в обсуждении результатов.

А. А. Попович – концептуализация идеи, определение цели работы и ее задач, участие в обсуждении результатов.

Received 03.07.2023

Revised 13.09.2023

Accepted 18.09.2023

Статья поступила 03.07.2023 г.

Доработана 13.09.2023 г.

Принята к публикации 18.09.2023 г.